FINAL REPORT

Supported under Grant No. NSG-2068

A.F. Charwat and M.E. Fourney

HOLOGRAPHIC FLOW VISUALIZATION

November 1976
Report No. UCLA-ENG-76105

UCLA . School of Engineering and Applied Science, Los Angeles, California

UCLA-ENG-76105
November 1976

HOLOGRAPHIC FLOW VISUALIZATION

by

A. F. Charwat and M. E. Fourney

FINAL REPORT

Prepared for NASA
Grant No. NSG-268

Mechanics and Structures Department

School of Engineering and Applied Science

University of California

Los Angeles, California

I. Introduction

The study of aircraft wakes is currently a pressing problem in aerodynamics because of the dangerous rolling moments suffered by aircraft which may penetrate the wake of preceeding aircraft, particularly during landing and takeoff. The problem has been under intensive investigation with regard to its various aspects: far-field vortex structure and decay, near-field rollup of the wing vortex sheet, stability, interaction, and coalescence of vortices their "meandering" under the influence of ambient gusts and turbulence and the practical problem of influencing the structure of the wake by adjustments in the wing lift distribution and spoilers or flaps to introduce concentrated turbulence and vorticity discontinuities into the wake. The bibliography dealing with this subject has become extensive. Reference 1 which describes the most recent underwater towing tests is the most directly applicable to the research envisaged here; additional references are given in that paper and need not be repeated.

The study of the vortex-sheet rollup as a function of the broad range of possible modifications in the wing geometry, including flaps, spoilers, engine exhaust, jets, etc. poses particularly difficult experimental problems and underscores the need for an accurate, convenient and economical means of visualizing the fine structure of the wake. Methods of direct flow visualization have always been useful and are often essential in the study of such complex flows, and particularly, in guiding attempts to optimize their configuration. However, clear flow visualization is not easily implemented. Obviously, none of the methods which rely on

interactions of the flow with diagnostic radiation traversing it, such as schliren, interferometry or light scattering and absorbtion are applicable because of the asymmetry and three-dimensionality of the field. Dye or smoke injection do not yield satisfactory results because of turbulent diffusion of the dye. Conversely, a clear record of the motion of neutrally buoyant, evenly distributed tracer particles can yield a complete and accurate picture. The flow can be seeded with scatterers relatively easily, particularly in water. However, in a flow as complex as a multi-vortex wake, the eye has difficulty following and interpreting the information in real time. Simple photography loses the essential three-dimensional information. The success and usefulness of particle-tracer visualization would be enhanced immeasurably by the development of movie-holography which stores and reproduces the full three-dimensional visual information. In addition, the method lends itself to subsequent quantitative reduction of selected records in terms of three-dimensional components of the local velocity field at all points of the flow.

Holograms of tracer particles in fluid flows have been obtained and discussed in research literature. Thompson, et al (2) developed a holographic technique for studying the size distribution of fog droplets. Fourney, et al (3) extended the technique by using a time sequence of holograms to determine size, velocity and spatial distribution of particles in a two-phase air-water flow. Many other investigators have utilized the technique to study various problems, among them Shofner, et al (4) who utilized

the technique to measure turbulence in a fluid by seeding it with relatively small particles (110μ). He reported an inability to determine the position of a specific particle in the direction perpendicular to the hologram to better than ±1 mm. However, Lee, Fourney and Moulton (5) showed that this was due to the limited numerical aperture and that diffraction limited resolution could be obtained by the technique and a particle could be located in this direction to within 20μm.

Other investigators, for example Wurker, et al (6) used the technique to study drop size distribution in liquid propellant rocket engines. In their studies the major difficulties resulted from the high droplet density. The upper limit found in Reference 7 was 1.5×10^4 particles/cm^3 (for a size distribution where 92% of drops are between 10-20μ diameter). However, this limit is far in excess of that to be used for seeding purposes in this study.

The full potential of the method for flow visualization, in particular, motion-holography (holographic movies) is yet to be developed. This, and its application to the aircraft wake problem is the subject of the present program.

II. Description of the Research Accomplished

The research has as an objective the development of holographic visualization of the vortex-wake of a lifting wing which will then be applied to the study of the influence of wing configuration on the vortex-sheet rollup.

The objectives stated in the original proposal were modified in discussions with the contract monitor: instead of aiming at the visualization of the vortex-wake of a towed model of an aircraft, it was agreed to emphasize testing of a model of a wing in our 4 x 12 inch water-channel. Instead of focusing on the rollup of the complex vortex-wake, we decided to pursue a more basic study of the velocity field and decay of a simple trailing vortex pair.

These changes led to an increased concern with the quality of the flow in the water-channel (which originally had been intended to serve only as a test-bed for the development of tracer particle holography). Early tests in the existing channel showed that because of its small cross-sectional size and relatively high turbulence level we could not maintain a "clean" trailing vortex. It turned out upon disassembly of the facility that previous research during which salt-water solutions were used in the channel resulted in substantial corrosion of the facility. In view of this, it became necessary to rebuild an entirely new water-tunnel. The School of Engineering granted us additional funds ($15,000) for the purpose, at no cost to the grant.

The design and construction of the water tunnel was completed. It is shown on Figure 1 and described in more detail below. The multiple-pulse laser system and associated holographic optics were

developed and tested. Holograms of tracer particles in water can now be taken routinely. This part of the research is described in more detail in the following section.

A theoretical study of the motion of tracer particles in vortical flows and the development of a novel liquid-drop tracer generator are also described in the following. Early experiments with quanine crystals, aluminum flakes and hollow micro-balloons showed the importance of the tracers for the success of the holographic visualization; in particular, the relative density of tracers (having a size appropriate for visualization) is important in the study of vortical flow where particle residence times are long.

These unexpected difficulties with the development of the facility and the technique lead, unfortunately, to time and cost overrun. During the period of the grant we have only been able to complete the preparatory work, some of which is original research, but which does not fully satisfy the initial objective. We are continuing (without funding) to calibrate and improve the overall facility and plan to seek at an early date the support necessary to proceed with the research plans originally stated in which is now a proven and fully operational facility.

II. The Water Tunnel

The new water tunnel (Figure 1) operates in a closed circuit. A large auxiliary storage reservoir permits emptying the test section without having to discard the test fluid (which is water deaerated and purified to prevent the deposit of films on the optical windows and cavitation); this also permits convenient filtering out of tracer particles as they accumulate in the circuit during visualization tests.

The tunnel has a nominal test section cross-section of 12 x 12 inches, 16 ft. long. The flow cross-section is compensated for boundary layer displacement effects. Four pairs of three-foot long side windows permit access at all streamwise locations and/or mounting of models. Plate glass windows are available for optical studies of the flow. The parallelism of the side walls and axial alignment of the tunnel were given careful attention.

The flow is driven by an 18 inch modified ship propeller and an electric motor with a Varidrive transmission. The power-section is vibration mounted and insulated from the tunnel circuit. The maximum design flow velocity in the tunnel is 15 ft/sec. Downstream of the test section the tunnel is vented to atmosphere through a stand-pipe which extends 5 ft. above the test-section centerline. This determines the mean test section pressure as well as the head of water at the propeller station (12 ft. of head).

The inlet nozzle contraction ratio is 16:1. The settling chamber is exceptionally large (4 ft x 4 ft x 8 ft long). The chamber has provisions for extensive turbulence management honeycombs, filters and screens. At the inlet to the test section there is a

large-resistance PVC foam filter (Scott foam, 10 pores per inch, two inches thick) supported by a stainless-steel screen stretched on a frame. Immediately ahead of the filter, an opening (stand pipe) across the entire top of the chamber is provided for a closed air-chamber resonator to absorb low frequency fluctuations and surges in the circuit. 12 inches downstream of the filter there is a flow strengthening honeycomb (1/8 inch cells, 9 inches long). Both the filter and honeycomb sections are recessed into the walls so as to maintain a uniform cross-sectional area; provisions are made (and continually being improved) to maintain the filters and honeycomb flat and uniform. The remainder of the settling chamber downstream of the honeycomb can accommodate additional turbulence-management screens. The optimal number, fineness and spacing of these screens remain to be determined, particularly if the tunnel is to be developed further for minimum turbulence level. With the basic arrangement: filter, honeycomb and a single screen spaced 1 ft. downstream of the honeycomb. The turbulence level in the test section is about 1% at 10 ft/sec (preliminary results) but we are confident that it can be reduced much further.

The tunnel test section is manufactured of plexiglass (with glass windows) in four carefully doweled and matched sections. The rest of the tunnel is entirely lined with bonded plastic (PVC) which is externally framed as needed with lumber and marine plywood. The honeycomb (aluminum) is coated with resin. With this construction we hope to have eliminated corrosion problems and minimized spurious electrical disturbances to hot film and hot wire instrumentation.

Thermal expansion with which we had problems at the outset is absorbed by a plastic bellows connecting the inlet to the convergent nozzle and the settling chamber and a rubber diaphragm junction between the test section and the downstream return leg. The test section inlet is rigidly held to the laboratory frame. The 16 foot test section rests on roller bearings on a steel T-beam structure which allows it to expand in the downstream direction. The support structure is designed for a maximum deflection under load of 0.001 inch; the bearing-plates are spaced two feet apart.

IV. Description of Holographic Technique

Holographic techniques have been used for several years to study two-phase flows and/or aerosols. The small liquid droplets in a gas phase lends itself to analysis by means of optical techniques. High magnification required to observe these droplets results in a small area of observation and very small depth of field when conventional optical methods are used. The advantages of holographic recording a volume of particles for later analysis has been described in detail in References (3) and (5). The technique can be directly applied to two liquid phases so long as the index of refraction difference between the two is sufficient to cause scattering from the droplet phase of a magnitude which will allow a hologram to be recorded.

The basic scheme is shown in Fig. 2. During the recording procedure the droplets are back illuminated by a ruby laser. The forward scattered light from each droplet acts as the information beam in the holographic process, while the light which is not scattered forms the reference beam. The reconstruction portion of this in-line holographic scheme consists of viewing the volume image through a microscope as shown in Fig. 2.

One of the major advantages of this scheme is the possibility of using effective large apertures.

Matkin et al (3) reported some difficulties using the holographic techniques due to the limit of resolution and the large focal depth of the reconstructed image. These difficulties can be substantially improved by using a large aperture in the holographic system. This is analogous to the use of small f/number stops in ordinary microscopy.

Rayleigh criteria is one of the typical expressions used to express the limit of resolution in ordinary optical systems.

$$\beta = 1.22\lambda/D$$

This equation states the well-known fact that for classical optics the resolution is inversely proportional to the aperture size. This is also true for holography since the holographic process can be considered as a process which merely freezes the optical wave front at a particular instant. Any process that is then performed in the wavefront to extract information will be limited by the laws of ordinary optics. Stigliani et al. (8) have experimentally and theoretically studied these relationships including the effects of the film. These studies involved the minimum size particles that could be clearly imaged by the holographic technique. Also Bieringer and Ringlien (9) showed an excellent reconstruction of objects of a few micron sizes using a large aperture. Their results are confirmed by the above statement.

Meier (10) also has shown that the focal depth is limited by diffraction in holographic procedures in an identical manner to that of ordinary optics, and his relationship follows

$$\Delta z = 2f_{NO}^2(1/\alpha)\lambda_1$$

The above equation states that the focal depth is proportional to the square of the f/number. The less the focal depth the more critical the focusing becomes. This then results in less uncertainty about the drop size and its location. Locating the drops more accurately will improve the accuracy of the velocity determination.

As one goes to lower f/number optics the cost increases. However, large apertures in holography can be easily achieved by moving the holographic plate close to the volume being sampled in order to include the light from a large scattering angle.

Due to scattering properties of small drops the light intensity falls off very rapidly as the scattering angle is increased. Since the photographic film used requires light of a certain intensity there is an angle beyond which one cannot operate. This will define the f/number. This point of cutoff is a function of drop size, the film characteristics, and the method of illumination. Fortunately, the cutoff angle increases with decreasing drop diameter.

General formulas for computing the location and magnification of reconstructed images have been derived by Matkin (3). Since a microscope was required to magnify the image, the recording and reconstruction of holograms were always made such that the conjugate real image could be observed. The location and magnification of conjugate real images are given by

$$b'_{ic} = \frac{\lambda_1 a a' b_i}{\lambda_2 a'(a-b_i) - \lambda_1 a b_i}$$

$$m_{ic} = \left(\frac{-a}{-a + b_i}\right)\left(\frac{-a' + b'_{ic}}{-a'}\right)$$

where

a = distance from hologram to recording source

b = distance from hologram to object

λ = wavelength

( )' ~ denote reconstruction

$( )_c$ ~ denote conjugate image

V. Results of Holographic Recording

The preliminary holographic work was performed by taking holograms of 25μ glass spheres supported on a thin glass slide with the He-Ne gas laser. Since a complicated calculation was required to determine the exact aperture, for the sake of convenience the distance from the object to film plane was expressed as the relative aperture. Figure 3 of Reference 5 clearly demonstrates that the resolution of the reconstructed image is improved as the aperture is increased. Considering the arrangement of the critical flow equipment and the comparison of the reconstructed images for the different apertures, it was decided to use 5.08 cm (2 in.) as the distance from object to film plane.

The average size of the glass sphere is 25μ diameter in the reconstructed images, but the smallest glass sphere shown is less than 10μ. This image has distinctive boundaries indicating that the holographic technique can record drops of only a few micron diameter.

The other purpose of using a large aperture technique was to shorten the focal depth for the reconstructed image so that the location and the velocity and/or position of the drop could be determined more accurately. The focal depth of the reconstructed image was determined from the error caused by refocusing the same image several times, and it was found that the focal depth was less than 10μ. An excellent example of the short focal depth achieved by this technique is shown in Figure 4 of reference 5 which consists of reconstructed images from a triple pulse exposed hologram of air-water two-phase flow. Figure 4 shows that the first two images are in focus and the third is out of focus in one phase and that the first two images

are out of focus and the third is in focus in other plane. The distance between these two image planes was 20μ.

Application to Liquid-Liquid Two Phase Flow

The extension of the results outlined above to liquid droplets in a liquid flow follows directly with only one complication. The index of refraction difference between the two phases must be sufficiently large to generate enough scattered light that a hologram may be recorded. Various types of particles, and particle generators have been experimented with, as detailed in previous sections of this report. Examples of the results are shown in Fig. 5 of the appendix. This appendix details the results of the work done with liquid-liquid two-phase flow.

Description of Multiple Q-Spoiled Ruby Laser System

To make multiple-exposed holograms which form the basis of the visualization system, it is necessary to have a laser with the ability to produce many Q-spoiled pulses. The exposure times necessary to produce a hologram of a moving particle is on the order of 50 nsec. Holographic films are typically very slow, therefore intense light pulses are required.

The following system descriptions of the ruby laser built for the purpose refers to circuit diagrams shown in Figure 3 and 4.

(a) Energy Storage System

The capacitor is charged by a voltage doubler circuit consisting of T_1, C_7, D_1, and D_2, with R_1 limiting current through the diodes

if the capacitor voltage reverses. The charging current is limited by C_u and the output voltage is regulated by limiting the pulses to the gate of the triac, TR-14. The capacitor can be discharged through the inductor into the flash lamps or into the energy dump resistors R-2, R-3 through safety relay RL-1. RL-2 disables the charging supply if the door interlock circuit is open or the over-voltage flip-flop is set. The status of this flip-flop is shown by the front panel LED. This flip-flop will also be set if the capacitor voltage goes above a level set on the over-voltage trimmer (now set to 3.7 kv).

(b) Energy Storage Logic

When the main power is turned on, the over-voltage flip-flop is set and disables the charging power supply. To charge the capacitor, turn on the H.V. power switch and push the reset button (or supply a +1 to +10 V pulse) and adjust the voltage with the left knob. Full pot rotation voltage can be set with the voltage trim pot (now set to 3.6 kv). To fire (the system will fire above 800 v) charge the capacitor and push the fire button (or supply a +1 to +10 v pulse).

(c) Laser Head

The two flash lamps are connected in series and located at the two outside foci in the polished aluminum double elliptical cavity. The center conductor of the power coax (green, .400 inch diameter) is positive and the lamp polarity must be maintained.

The trigger input to the laser head is a 0 to 2 v transition generated when the fire button is pushed. This signal can be used to synchronize an oscilloscope trace with the high voltage trigger

applied to the lamps.

Lasing threshold is about 1800 volts, about 625 joules, when properly aligned.

(d) Pockel Cell Circuit

The trigger signal starts a variable delay circuit, IC-7. After the delay, IC-5 and IC-6, a variable frequency oscillator drive the base of the avalanch transistor (Raytheon RT 333A). This transistor, and the recharge transistor, produce a series of -180 volt pulses that are inverted by the pulse transformer. These pulses are attenuated 20:1 to the monitor BNC on the laser head. The pulses drive the grid of tube V-1 (type 6LQ6). This is the upper tube with the grounded cathode.

The bias on the vacuum tubes is set for an idle current of 2 to 3 ma, monitored on the back of the upper chasis (1 V = 1 ma). To set this bias, slowly increase the Pockel cell voltage while monitoring the tube current. The bias pot is located on the small copper board on the laser head. Set the bias for 2 to 3 ma at 3.1 kv.

Operation of System

(a) Free Running Mode

Unit can be operated in free running mode by setting Pockel cell voltage to 0.

(b) Q-Spoiled Mode

The laser is Q-spoiled by means of a Pockel cell. The Pockel cell opens in less than 15 nsec and remains open for approximately 100 nsec, and closes with a fall time of approximately 150 nsec. The Pockel cell may be opened at a repetition rate of 100 Khz to

1 Mhz. The rate is controlled by rate adjustment pot on a laser head. Exact rates must be determined by monitoring BNC test point at laser head. This is 50-ohm impedance, approximately +8 volt, 50 nsec duration pulse. The Pockel cell operation may be delayed from 100 μsec to 1.5 msec after initiation of trigger pulse. This delay is controlled by pot on laser head. The delay gate period must be monitored at pin #9 on 72710 IC. This gate period is a square wave of +2 v for duration of Pockel cell operation. An alternate method is to observe the monitor test point; however, this requires a fast scope.

To obtain a string of equal amplitude pulses requires an energy balance between flash lamp input and lasing output. Since the lasing efficiency of the ruby is a function of its temperature, a trial and error operational procedure with timed intervals must be established.[1]

[1]For further details see M.E. Fourney Ph.D. Dissertation, Calif. Inst. of Tech., 1963.

References

1. D.L. Ciffone and K.L. Orloff. Far-Field Wake Vortex Characteristics of Wings. Ames Research Center, NASA preprint to be presented at the AIAA Meeting, Palo Alto, California, June 15, 1974.

2. Thompson, B.J., et al., J. Appl. Meteor., 5, 434, 1966.

3. Fourney, M.E., Matkin, J.H., and Waggoner, A.P., "Aerosol Size and Velocity Determination Via Holography," The Review of Scientific Instruments, 40, 205, 1969.

4. Shofner, F.M., et al., AFFDL-TR-68-140, 1968, and AFFDL-TR-69-100, 1970.

5. Lee, Young J., Fourney, M.E., and Moulton, R.W., "Determination of Slip Ratios in Air-Water Two-Phase Critical Flow at High Quality Levels Utilizing Holographic Techniques," AIChE Journal Vol. 20, No. 2, March 1974.

6. Wuerker, R.F., et al., AFRPL-TR-69-204, 1969.

7. Stigliani, D.J., Jr., Mittra, R., and Semonin, R.G., "Particle-Size Measurement Using Forward-Scattering Holography," J. Opt. Soc. Am., 60, 1059, 1970.

8. Bieringer, R.J., and Ringlien, J.A., "Diffraction-Limited Holography," Appl. Opt., 10, 1632, 1971.

9. Meier, R.W., "Depth of Focus and Depth of Field in Holography," J. Opt. Soc. Am., 55, 1963.

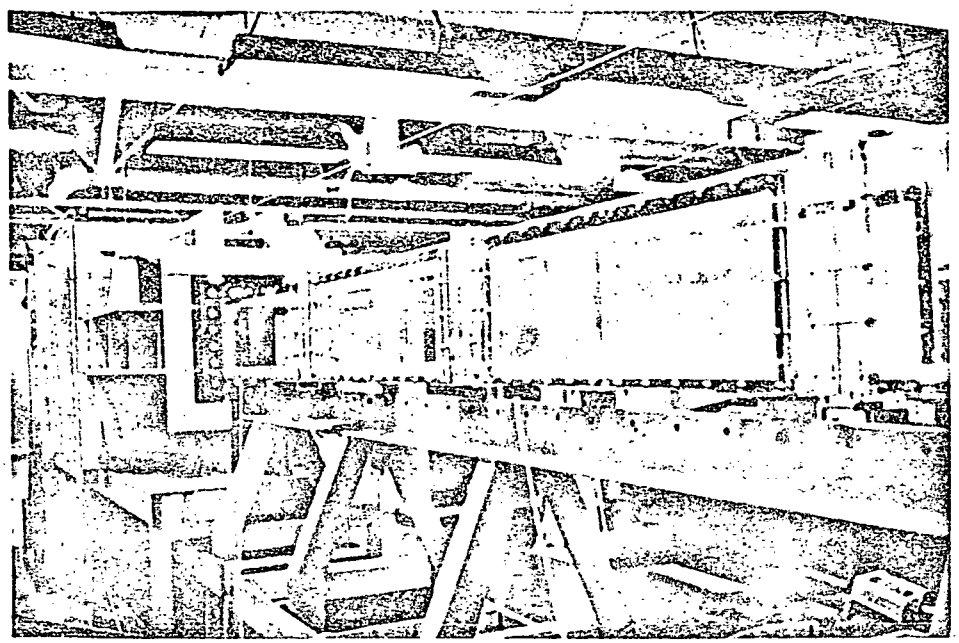

WATER TUNNEL TEST SECTION VIEWED FROM DOWNSTREAM

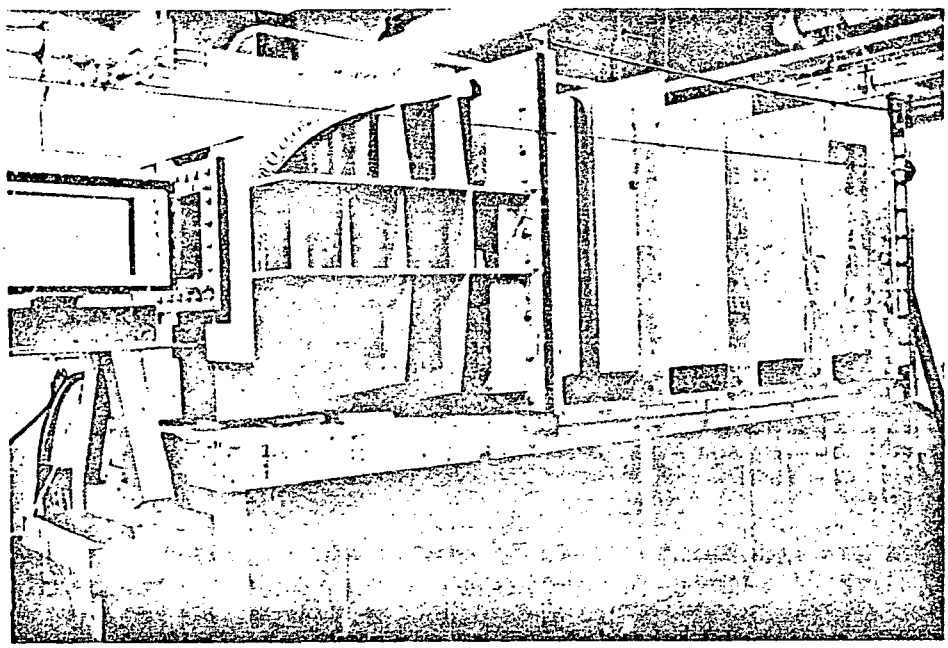

SETTLING CHAMBER AND INLET

Fig. 1. The UCLA Water Tunnel

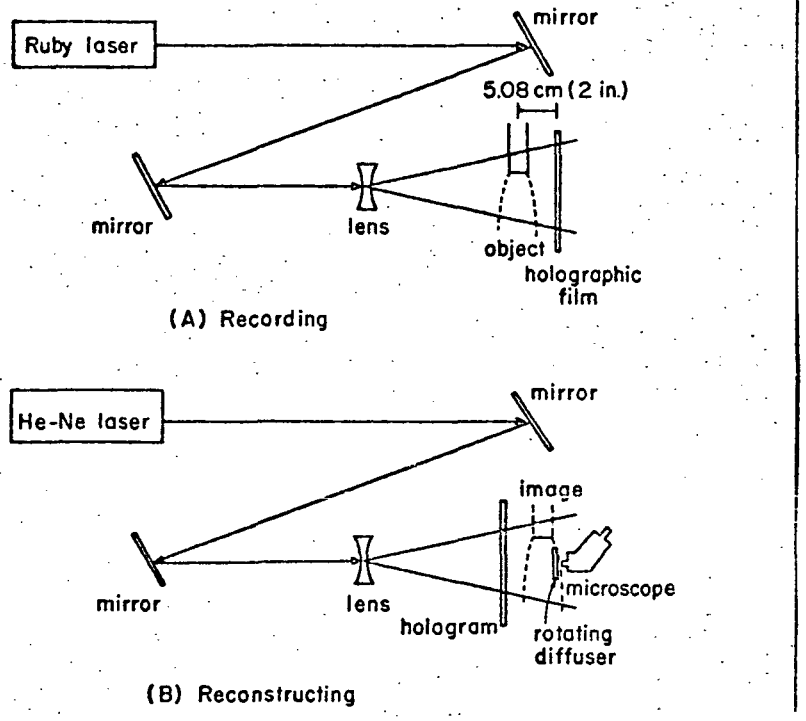

Fig. 2. Arrangement for Recording and Reconstructing Holograms

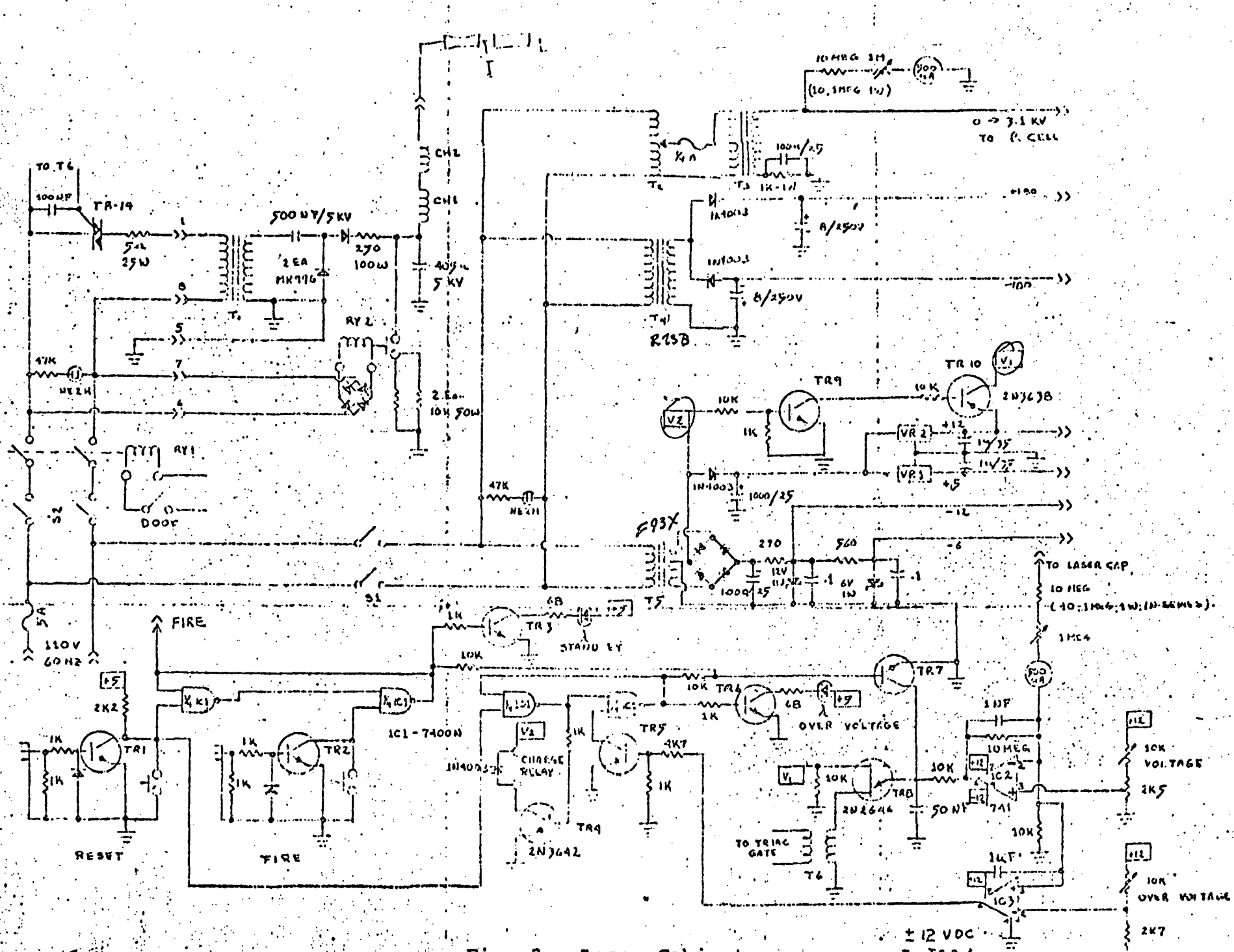

Fig. 3. Laser Cabinet

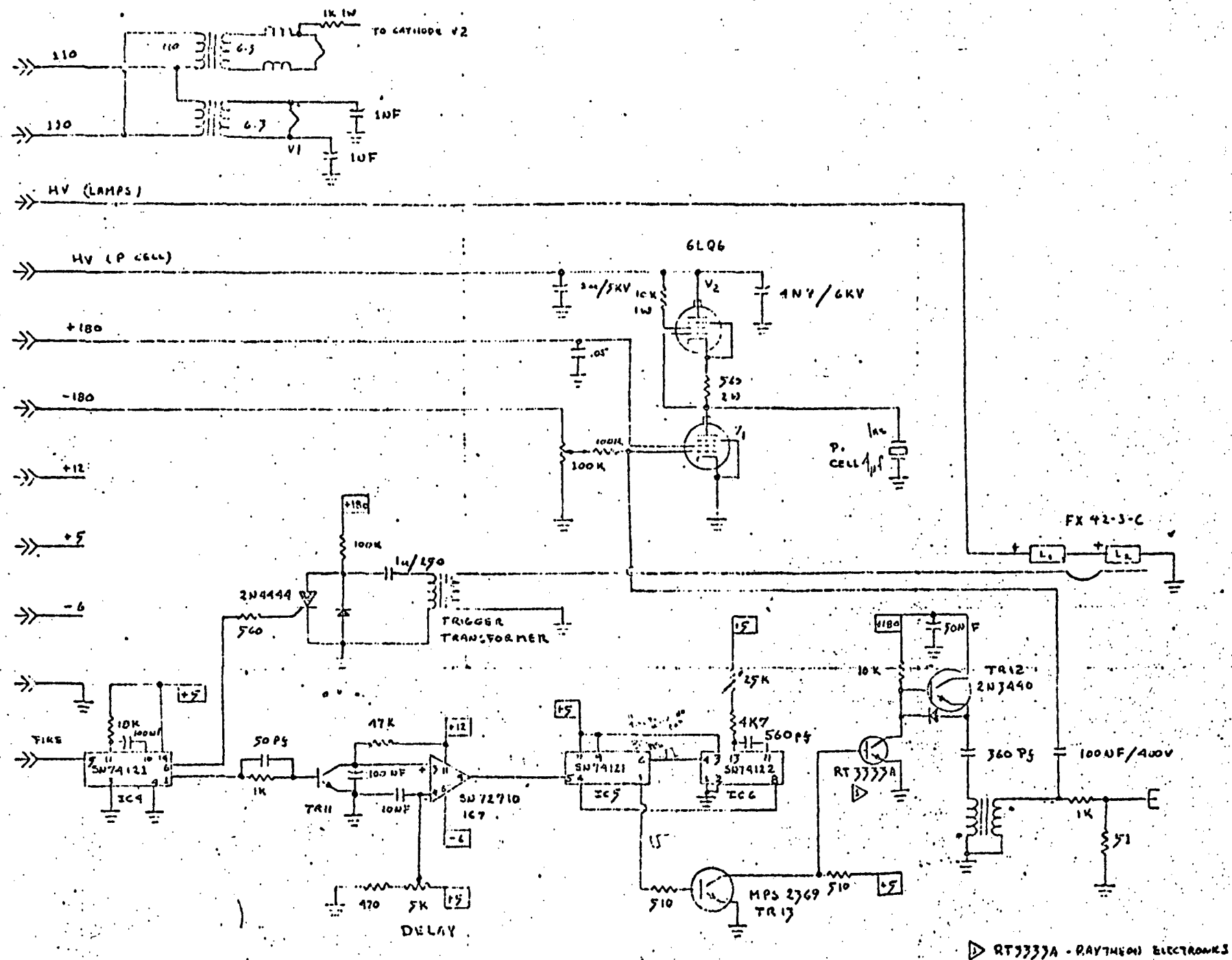

Fig. 4. Laser Head

APPENDIX A

The Generation and Motion of Near-Neutrally Buoyant Tracers for Holographic Visualization of Vortical Flows

Abstract

Holograms of tracers injected into complex flow fields provide a way of visualizing the structure of the flow and simultaneously provide a quantitative record of the complete three-dimensional velocity field. A practical application of this technique to water-channel testing requires the use of relatively large tracers which must then be neutrally buoyant to follow the flow. This paper describes the design and performance of a tracer generator using droplets of a mixture of liquids the density of which can be accurately matched to that of the ambient fluid. An analysis of the motion of particles of arbitrary density and size in solid body and potential vortex flows is presented.

Introduction

Streakline-visualization is a useful diagnostic tool in the study of complex flow fields. It allows one to gain an understanding of their overall structure and identify the particularly significant regions for further probing. Unfortunately, truly complex, three dimensional, highly turbulent flows where visualization could be most useful are the most difficult to visualize. Smoke and dyes diffuse rapidly and if the flow is unsteady (or contains high, large scale turbulence) only discrete particle-tracer techniques can be used. Examples of such flows of considerable current interest are the vortex-wake downstream of lifting wings or the wakes generated by irregular obstacles in a shear-flow, such as buildings in the wind-boundary layer.

The potential of particle tracer visualization is greatly enhanced by the development of laser holography. It is not only a way to visualize the structure of the flow but also a precise quantitative tool capable of yielding data on the local, instantaneous, three dimensional vector velocity field. A double-exposure hologram with a properly chosen interval between exposures provides a record of the position of the tracer particles at two instants in time. The displacement of each tracer between exposures in the plane of the film yields the local velocity components in that plane, like in ordinary photography. A hologram contains, in addition, information on the displacement of the tracers along the optical axis. This information is extracted by viewing the hologram through a small depth-of-field optical system (a microscope). Figure 1 shows, as an example, two microphotographs of a hologram of

a pair of tracers. The microscope is focused on one and on the other particle, respectively. The change in focal adjustment is proportional to the distance between the particles "into" the picture. In the example shown here the tracers have a diameter of 200 microns and their spacing normal to the photograph is found to be 340 microns. Considerably finer spatial resolution is possible.[1][2]

The present study is concerned with the development of a practical tracer-particle generator for use in holographic flow visualization in water-tunnels, specifically, for the study of vortex wakes. This emphasis defines the desirable characteristics of the tracers, which are reviewed below.

The optical disturbances associated with taking holograms through glass windows into a water environment are considerably larger than in air. A series of experiments using tracer particles of various sizes ranging from 10 microns upwards proved that, whatever the optical arrangement, intensity of illumination and particle material, tracers smaller than 50 microns did not yield useful pictures. Their image could not be distinguished easily from "speckle patterns" and shadows resulting from nonuniformities in the glass windows and gradients in the flow. In order to maintain the value of this technique as a "visualization" technique, that is, in order to be able to view a hologram and clearly see the structure of the flow field with the naked eye, tracers of the order of 100 microns are necessary.

The tracers should be spherical. It is then possible to determine accurately when they are in focus, as illustrated in Figure 1.

We experimented with guanine crystals used in the cosmetic dye industry. These are platelets having typical dimensions of 30 x 1 micron and a very high refractivity. They are attractive as tracers because of their high drag to mass ratio; their irregular shape makes it difficult to determine when they are in focus; the uncertainty in determining their out-of-plane shift is an order of magnitude larger than for spherical particles of equal size.

The tracer particles must follow the fluid. This is usually insured by choosing small particles which have very high drag as compared with their inertia. Larger particles can follow the flow only if they are nearly neutrally buoyant; an analytical study of the motion of tracers of varying specific gravity in vortical flow is described in the text of this paper. Since it is virtually impossible to find solid particle tracers with an accurately controllable density, one is forced to consider tracers which are droplets of a mixture of liquids inviscible in water, the specific gravity of which could be matched exactly to that of the ambient fluid.

An unambiguous interpretation of double-exposure holograms requires that the average spacing between tracers in the field be significantly larger than the distance they travelled between exposures. If a typical diameter of the tracer is 100 microns and its typical displacement between exposures is set at a few particle diameters (which gives an excellent practical resolution of the velocity field) the seeding density should be of the order of one particle per centimeter; if typical flow velocities in water-tunnels

range from 1 to 10 meters/sec, the required rate of seed-particle injection is 100 to 1000 particles per second.

Last but not least, the particle generator must be sufficiently small to avoid disturbing the flow under study. Considering typical sizes of water-tunnel models, the characteristic size of the tracer injector must be of the order of half a centimeter.

The Design of the Drop Generator

A considerable number of designs of drop generators have been reported in the literature. None of these designs meets all the constraints discussed in the Introduction. The two general types are: (a) Generators producing a fine liquid jet and relying on the Rayleigh instability of the jet to disintegrate it into drops. This principle is mainly used to produce aerosols but it has also been applied to the generation of liquid drops in a liquid environment[3]. Generators of this type tend to be high frequency devices. (b) Generators using some mechanical means to shear off small masses of liquid: rotating blades[4], vibrating reeds and wires[5], pulsating supply pumps[6] and many others (the references quoted here are by no means a complete bibliography but merely typical examples). These devices can be made to produce drops of the size and low frequency contemplated here but they tend to be physically very large.

In the present design the tracer liquid is injected through a small hypodermic needle and sheared off into droplets by a relatively strong, coaxial jet (of ambient fluid) surrounding the injector tip. The generator is sketched in Figure 2. The central

tube is a stainless steel hypodermic with 102 microns (.004 inches) I.D. and 204 microns O.D. The diameter of the coaxial jet is .95 mm. The overall dimensions of the injector head are 2.5 mm O.D. and 5 mm in length.

The tracer liquid is a mixture of a mineral oil (the usual "red fluid" used in manometers) and carbon tetrachloride. These fluids have specific gravities of 0.827 and 1.5, respectively. Experiments included mixtures in various proportions giving tracers with positive or negative buoyancies. The surface tension of the components (in water) is nearly identical: 48 dynes/cm for the oil and 45 dynes/cm for carbon tetrachloride. One can therefore expect no effects due to mixture ratio on the drop size, which was experimentally verified. Note that there are other mixtures which could also be used to produce a neutrally buoyant tracer, for example [7] benzine and carbon tetrachloride.

The size of the droplets formed by this method depends on a balance between surface tension forces and the drag exerted by the surrounding jet on the nascent drop; for near-neutrally buoyant drops gravity is absent. A spherical drop of radius R formed on a needle of radius r (with $R/r > 1$) and acted upon by a drag force $C_D \frac{1}{2}\rho V^2(R^2-r^2)$ is in equilibrium when

$$\frac{C_D}{4}\left(\frac{\rho r V^2}{\sigma}\right) = \frac{\frac{r}{R_0} - \frac{r}{R}}{\left(\frac{r}{R}\right)^2 - 1}$$

This model serves to define the governing parameters for scaling purposes. In actuality the fluid mechanics in the neighborhood

of the nascent drop is very complex, especially when $R < r$. The ratio $(\rho r V^2/\sigma)$ represents the surface tension contact angle involving the characteristic of the solid-liquid and liquid-liquid interfaces, but it is best interpreted as the equilibrium drop-to-tube radius when the drag force (or the ambient flow velocity) vanish. This can be determined experimentally, see Figure 3. This figure depicts a drop of pure mineral oil; the slight buoyancy force on it can be neglected. For the tracer liquids tested we obtained

$$.15 < \frac{r}{R_o} < .17$$

The performance of the coaxial-jet drop generator is shown on Figure 4. The generator can produce drops smaller than the outer diameter of the injector tube, in fact, smaller than its internal diameter. In that limit the simple model described above is clearly not applicable. Turbulence and instabilities of the base-flow around the end of the injector tube would seem to be responsible for "tearing" off the nascent drops before they grow to "equilibrium" size. Figure 5 shows typical photographs (of holograms) of the near-field. In particular, Figure 5A captures by a shadowgraph effect the turbulence in the secondary jet. Due to the relatively large focal depth of the camera, all droplets in the field are here approximately in focus, in contrast with the microscope picture, Figure 1.

We investigated some variations in the design which should affect the flow and pressure fluctuations in the immediate neighborhood of the injector-tube exit. One of them is the overhand of the in-

jector tube beyond the exit-plane of the control jet. Best results (most regular drops of small diameter) were obtained with an overhang of about one diameter of the jet. We also tried to introduce swirl into the control jet by threading the secondary flow passage (0.8 UNM miniature screw thread). The base pressure around a blunt coaxial cylinder in rotating flow[8] is known to be very low and the wake closes much more abruptly than in flow without rotation. These elements should contribute to an early "pinching" off of droplets. However, possibly because of the low thread-angle and depth, this did not measurably change the performance of the drop generator.

The operation of this injector is highly satisfactory. Drop sizes are controllable; they issue with good regularity. The drop size distribution is quire narrow, see Figure 6. The drops are spherical which makes focusing accurate. The optical properties of the droplets (lense-effect) are adequate to produce good photographic contrast without addition of dye. The coaxial control jet velocity decays reasonably rapidly (in a distance of the order of 10 jet diameters) so that the total disturbance to the flow is reasonably small. We feel that the injector could be easily fabricated entirely of stainless tubing (instead of the brass body used here) with a finer control jet and outside dimensions about half those of the unit tested. The overall disturbance to the flow can be assumed to decrease with the square of the jet dimension.

The Motion of Tracers in Vortex Flows

The equations of motion of particles in polar coordinates are taken to be

$$(1) \quad (\ddot{r} - r\omega^2) = -S\frac{1}{\rho_f}\left(\frac{\partial P}{\partial r}\right)_f + SB(u_f - \dot{r})$$

$$(2) \quad r\dot{\omega} + 2\omega\dot{r} = -\frac{S}{r}\frac{1}{\rho_f}\left(\frac{\partial P}{\partial \theta}\right)_f + SB(v_f - \omega r)$$

$$S \equiv \frac{\rho_f}{\rho_p} \quad ; \quad B \equiv \frac{9\nu_f}{2a^2}$$

The pressure gradient terms as well as the velocities u_f and v_f (radial and tangential, respectively) describe the flow in which the particle is imbedded. The pressure gradient term is an approximation to the force on the particle arising from the pressure distribution on its surface[9][10]. It is important in vortical flows which are dominated by the balance between centrifugal and pressure forces. The presence of this term leads to the result that a neutrally buoyant particle initially in equilibrium with a fluid vortex will continue to rotate with the fluid without slip, which is intuitively correct. Body forces due to gravity are neglected in this formulation. The drag force on the particle is assumed to be Stoksian. The drag parameter B is of the order of $10^3 sec^{-1}$ for typical particles (a = 100 microns) in water.

Two cases are discussed below for which the description of the fluid motion is the following:

(a) Solid body rotation

$$\begin{cases} u_f = 0 & ; \; V_f = \omega_f r = K_s r \\ \left(\frac{\partial p}{\partial \theta}\right)_f = 0 & ; \; \frac{1}{\rho_f}\left(\frac{\partial p}{\partial r}\right)_f = \omega_f^2 r = K_s^2 r \end{cases} \tag{3}$$

(b) Free (potential) vortex

$$\begin{cases} u_f = 0 & ; \; V_f = \omega_f r = \frac{K_p}{r} \\ \left(\frac{\partial p}{\partial \theta}\right)_f = 0 & ; \; \frac{1}{\rho_f}\left(\frac{\partial p}{\partial r}\right)_f = \frac{K_p^2}{r^3} \end{cases} \tag{4}$$

Tracers in a Solid Body Vortex

Substitution of equation 3 into (1) and (2) yields:

$$\ddot{r} + SB\dot{r} - r\omega^2 + SK_s^2 r = 0 \tag{5}$$

$$r\dot{\omega} + 2\omega\dot{r} + SB\omega r - SBK_s r = 0 \tag{6}$$

Define the variable q

$$q = \frac{\dot{r}}{r} \tag{7}$$

and use

$$\dot{\omega} \equiv \frac{d\omega}{dq}\frac{dq}{dr}\frac{dr}{dt} = \frac{d\omega}{dq}\left[\frac{\ddot{r}}{r} - \left(\frac{\dot{r}}{r}\right)^2\right] \tag{8}$$

to obtain from (5) and (6), respectively:

(9) $$\frac{\ddot{r}}{r} = \omega^2 - S K_s^2 - S B q$$

(10) $$\frac{d\omega}{dq}\left[\frac{\ddot{r}}{r} - q^2\right] = S B K_s - S B \omega - 2\omega q$$

So that, after rearrangement

(11) $$2\frac{dq}{d\omega} = \frac{\omega^2 - \left(q + \frac{SB}{2}\right)^2 + \left(\frac{S^2B^2}{4} - SK_s^2\right)}{\frac{SB}{2}K_s - \omega\left(q + \frac{SB}{2}\right)}$$

Figure 7 shows the character of the particle trajectories in the q-ω plane for the case in which $(SB/2) > \sqrt{S}K_s$, which is the more practical case. The solution for the other cases (the axis of the hyperbolas N = 0 is along q = BS/2) exhibits identical characteristics. Pluses and minuses in the various regions designate the sign of the slope of $dq/d\omega$ along the curves representing solutions. The direction of the trajectory (increasing time) is indicated by arrows.

Beginning from any point in the plane, which represents the initial conditions at the instant of its insertion in the flow, the particle will move towards a singular point marked A in the q-ω plane. In the physical plane this path corresponds to decaying oscillation about a spiral, assymptotic path, which is given by the values of $q = \dot{r}/r$ and ω at point A; explicitly:

(12) $$\frac{1}{\sqrt{S}K_s}\frac{\dot{r}}{r} = \frac{1}{\sqrt{2}}\left[\frac{S}{4}\left(\frac{B}{K_s}\right)^2 - 1 \pm \sqrt{\left[\frac{S}{4}\left(\frac{B}{K_s}\right)^2 - 1\right]^2 + \left(\frac{B}{K_s}\right)^2}\right]^{1/2} - \frac{\sqrt{S}}{2}\left(\frac{B}{K_s}\right.$$

(13) $$\frac{1}{\sqrt{S}K_s}\omega = \frac{1}{\sqrt{2}}\left[1 - \frac{S}{4}\left(\frac{B}{K_s}\right)^2 \pm \sqrt{\left[\frac{S}{4}\left(\frac{B}{K_s}\right)^2 - 1\right]^2 + \left(\frac{B}{K_s}\right)^2}\right]^{1/2}$$

It follows that the average radius of the particle varies exponentially with time at a rate which depends on the ratio of the fluid to particle densities and the dimensionless parameter B/K_s.

It is easily shown that when S = 1 the assymptotic motion of the particle is a steady rotation at $\omega = K_s$ (the singular point A lies at $\omega = K_s, q = 0$). When S > 1 (the particle is lighter than the fluid) q_A is negative ($\dot{r} < 0$) and it will move towards the center of the solid body vortex. The reverse occurs when S < 1.

The second singular point on Figure 7 clearly represents an unstable condition. It corresponds to injection of the particle with an angular velocity against the flow (negative values of ω). Any disturbance will cause the particle to spiral out of this point and follow the trajectory indicated towards point A.

Free Vortex Flow

For a potential vortex, one has by substitution of Equations (4) into (1) and (2)

$$\ddot{r} + SB\dot{r} - r\omega^2 + S\frac{K_p}{r^3} = 0 \tag{14}$$

$$r\dot{\omega} + 2\omega\dot{r} + SB\omega r - \frac{SBK_p}{r} = 0 \tag{15}$$

Multiplying the second equation by r it can be integrated

$$(r^2\omega) = (r_i^2\omega_i - K_p)\exp.(-SBt) + K_p \tag{16}$$

where $r_i^2\omega_i$ are the initial conditions at the injection of the tracer. The radial motion of the tracer is then described by

$$\ddot{r} + SB\dot{r} + \frac{1}{r^3}\left[(S-1)K_p^2 - C^2\exp(-2SBt) + 2K_pC\exp(-SBt)\right] = 0 \quad (17)$$

where $$C = (r_i^2\omega_i - K_p)$$

The effect of the initial conditions of injection decays exponentially in time. It becomes negligible if:

(a) The particle injection conditions are such that

$$r_i^2\omega_i = K_p = r^2\omega_f^2$$

(b) after sufficient time $t \gg SB$. Since for small tracers in water B is large (of the order of 10^{-3}) this case is practically significant. The time constant characterizing the decay of the initial disturbance $(SB)^{-1}$ should be compared with K/r_i^2: the ratio $K_p(r_i^2 SB)$ represents the number of revolutions required to attenuate the initial transient.

Under these conditions (which do not in any case change the general character of the solution) Equation 17 reduces to

$$\ddot{r} + SB\dot{r} + \frac{1}{r^3}(S-1)K_p^2 = 0 \quad (18)$$

or

$$\frac{d\dot{r}}{dr} = \frac{K_p^2(1-S) - SB\dot{r}r^3}{\dot{r}r^3} \quad (19)$$

Figure 8 shows the character of these solutions in the $\dot{r}, r$ plane for both S smaller and larger than unity. Arrows indicate the direction of motion in time. As in the solid body vortex particles heavier than the fluid ($S > 1$) will move outward while

lighter particles will move towards the center. For neutrally buoyant particles, S = 1, Eq. 18 can be immediately integrated, showing that neutrally buoyant particles in a free vortex will also reach equilibrium with the flow at some radius (which differs from the injection radius depending on the initial conditions) regardless of the injection velocities.

Conclusion

A significant conclusion of this study is that the motion of a particle in either a solid-body or free vortex will converge to full equilibrium with the fluid regardless of the initial disturbance at the injection of the particle, provided that the particle is neutrally buoyant. Conversely, when the particle has a density different (smaller or larger) than the ambient fluid, it will always move (inward or outward, respectively) relative to the flow. The relative motion becomes asymptotically independent of the initial conditions; the error can be estimated from a numerical solution of equations given in the text.

The idea of producing liquid-droplet tracers whose density and size is finely controllable seems feasible. The performance of the coaxial-jet generator outlined in the text is very satisfactory for the purpose.

Acknowledgment

This work was performed under sponsorship of NASA (Grant NSG 206B). Holographic equipment was provided by Prof. M. Fourney, whose contribution is gratefully acknowledged. Thanks are due to Prof. J. Cole for his help in the analysis of the particle motion and to Messrs. D. Alliskievich and Gary Firment for assistance in the laboratory.

List of References

1. Fourney, M.E., Matkin, J.H. and Waggoner, A.P., Rev. Sci. Instr. 40, 205, 1969.
2. Lee, Y.J., Fourney, M.E., Moulton, R.W., Am Ch E Journal 20, No. 2, March 1974.
3. Smith, S.W.J. and Moss, H., Proc. Roy. Soc., A93, 373, 1917.
4. Ratner, A.C. and Haliburton, W., Rev. Sci. Instr. 25, 1124, 1955.
5. Wolf, W.R., Rev. Sci. Instr. 32, No. 10, pp. 1124-1129, October 1961.
6. Atkinson, G.W., Miller, . ., Rev. Sci. Instr. 36, p. 846, 1965.
7. Kalinske, K. and Paen, D., Ind. Engr. Chem., 36, p. 222, 1944.
8. Charwat, A.F. and Schlesinger, M.E., Astronautica Acta 17, pp. 375-386, Pergamon Press, 1972.
9. Drew, D.A., Phys. of Fluids, 17, No. 9, pp. 1688-91, Sept. 1974.
10. Drew, D.A. and Segal, L.A., Stud. Appl. Math., L3, 205, 1971.

List of Figures

Figure 1. Determination of the out-of-plane displacement of tracers from a hologram.

Figure 2. Design of coaxial jet drop generator.

Figure 3. Drop forming with no coaxial control jet. Mineral oil, s.g. 0.827.

Figure 4. Performance of the drop generator.

Figure 5. Typical operation of the tracer generator. Top: R = 180 microns; bottom: R = 310 microns (photographs of hologram, large depth of field).

Figure 6. Typical particle size distributions.

Figure 7. Character of the solutions for the motion of particles in a solid-body vortex.

Figure 8. Characteristic trajectories of particles in a potential vortex.

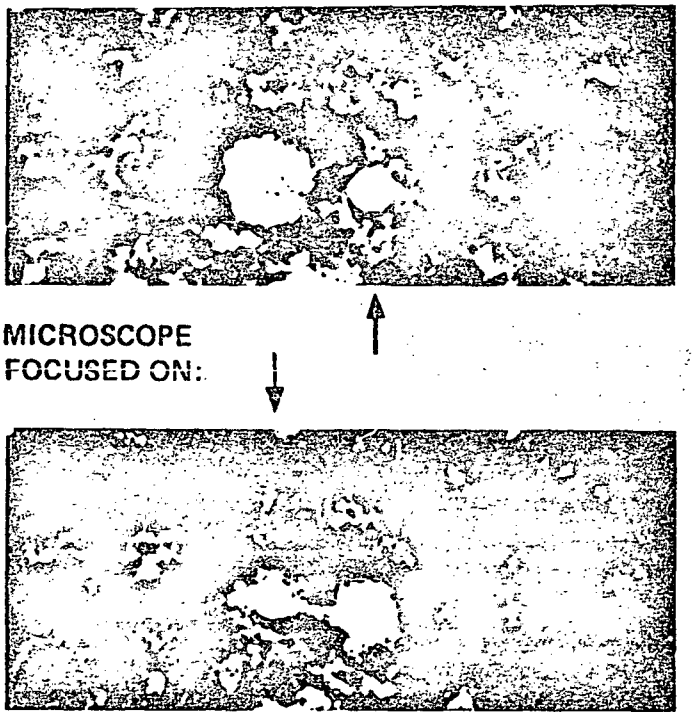

Figure 1. Determination of the out-of-plane displacement of tracers from a hologram.

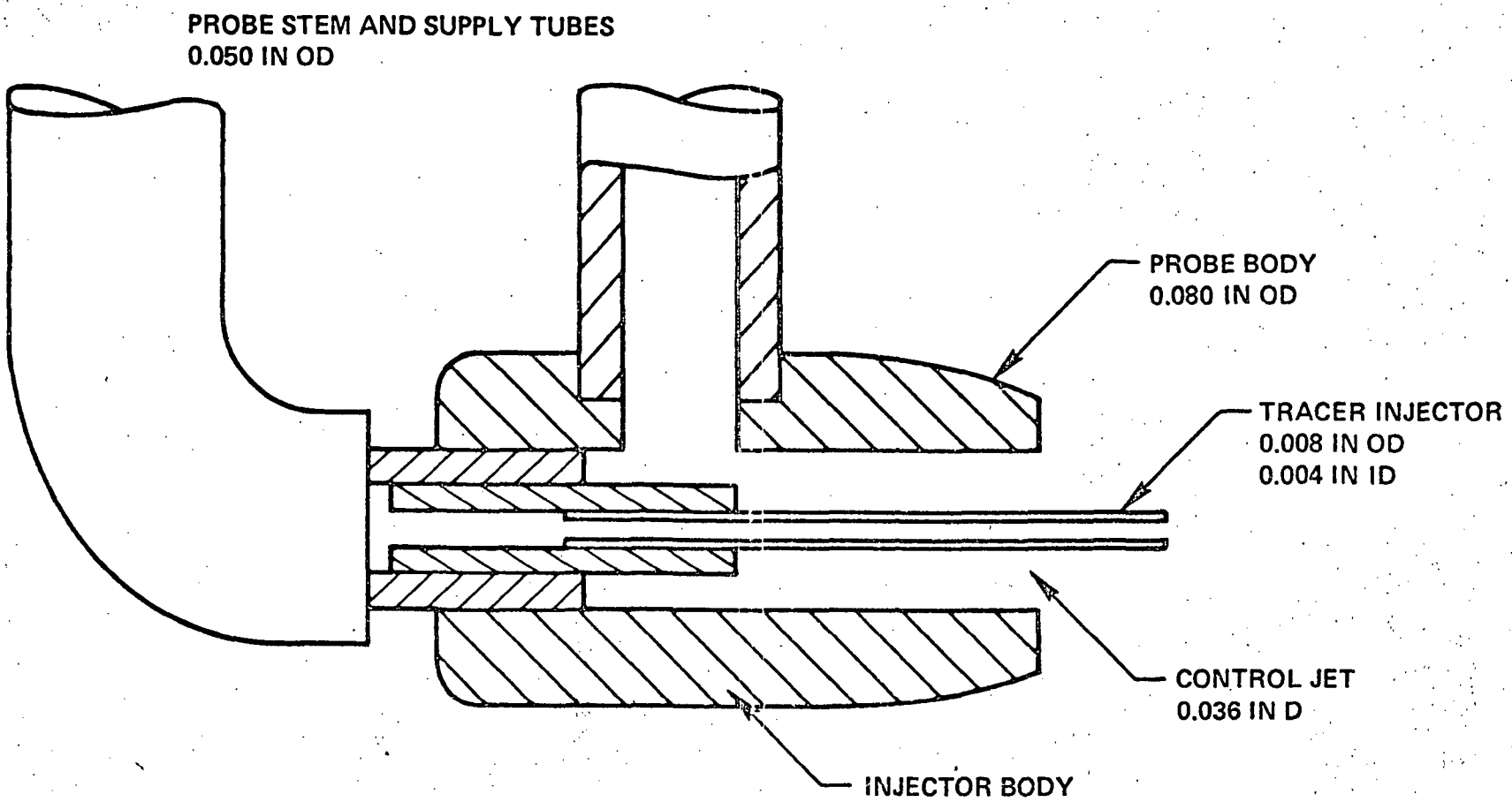

Figure 2. Design of coaxial jet drop generator.

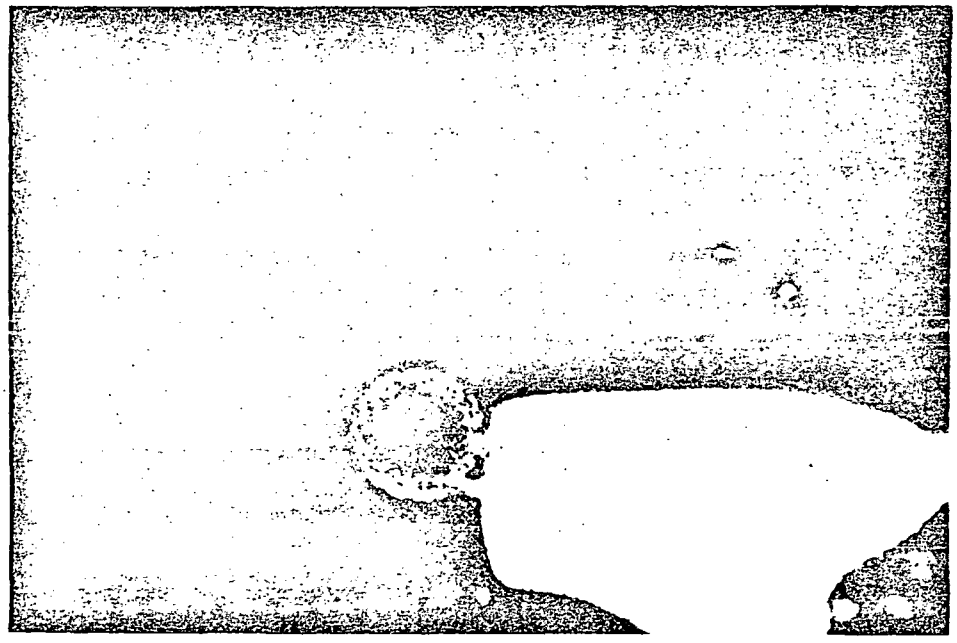

Figure 3. Drop forming with no coaxial control jet. Mineral oil, s.g. 0.827.

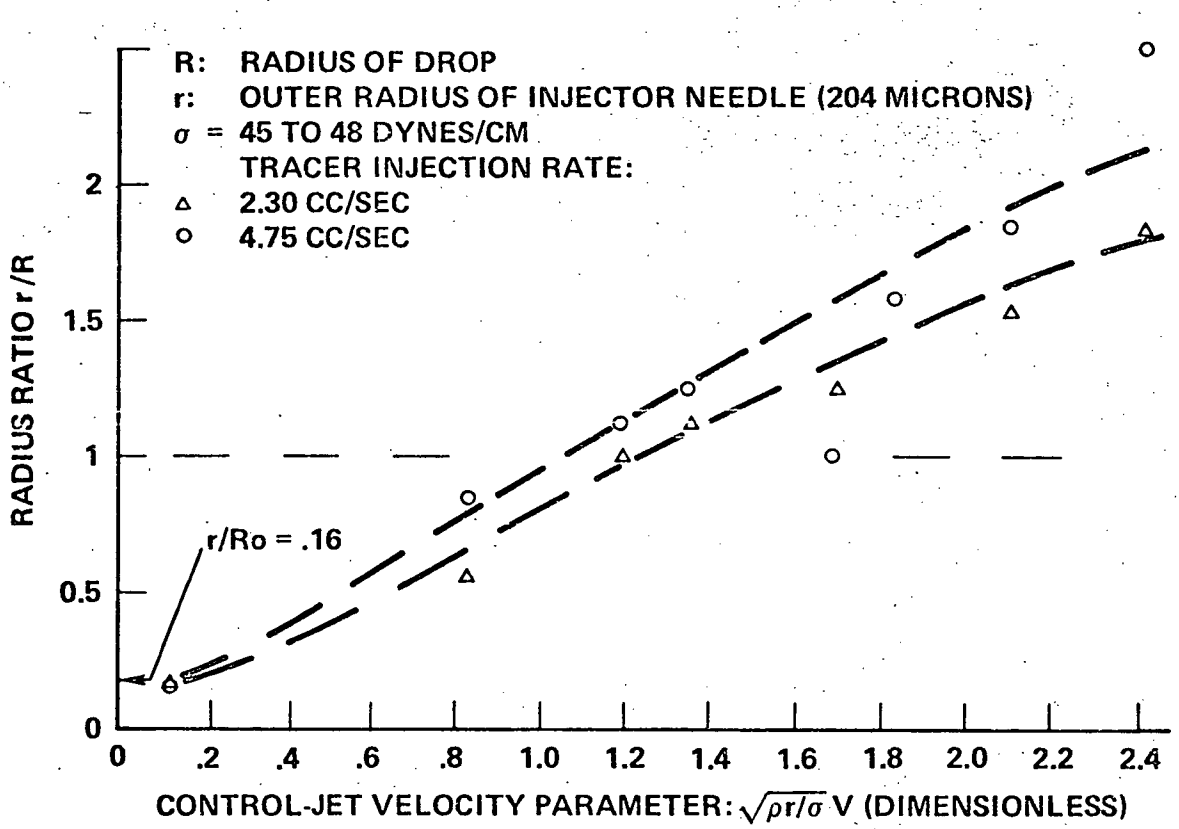

Figure 4. Performance of the drop generator.

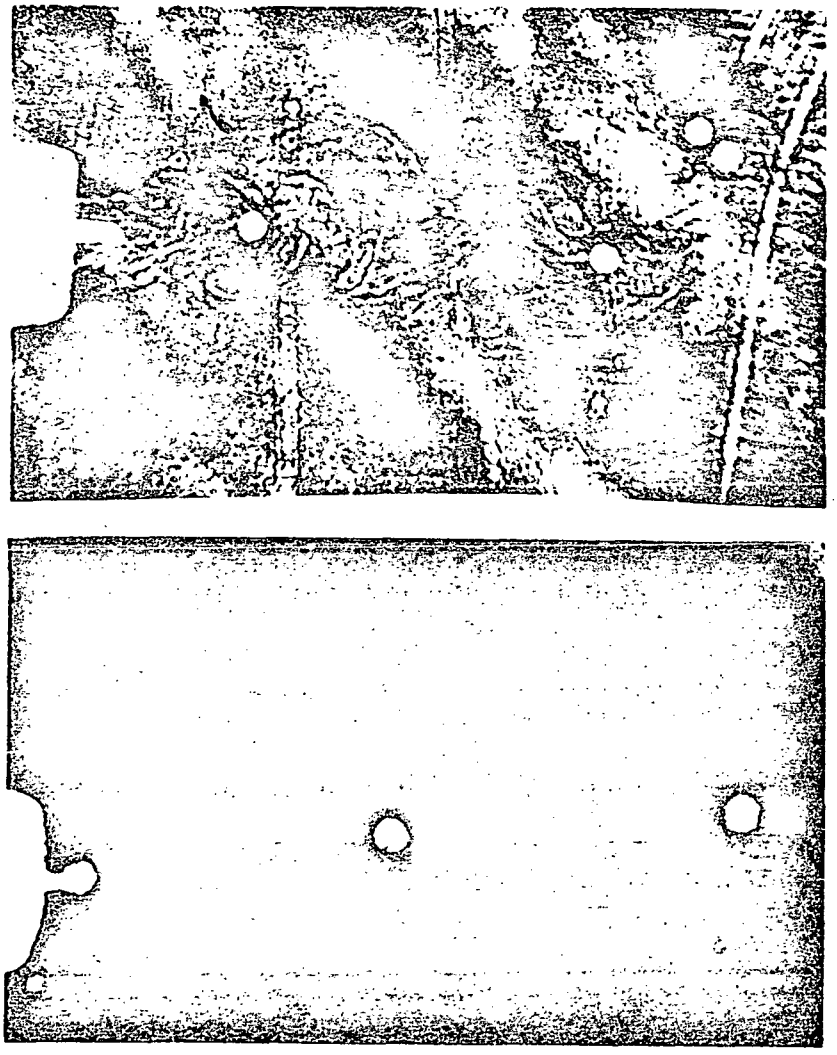

Figure 5. Typical operation of the tracer generator. Top: R= 310 microns (photographs of hologram, large depth of field).

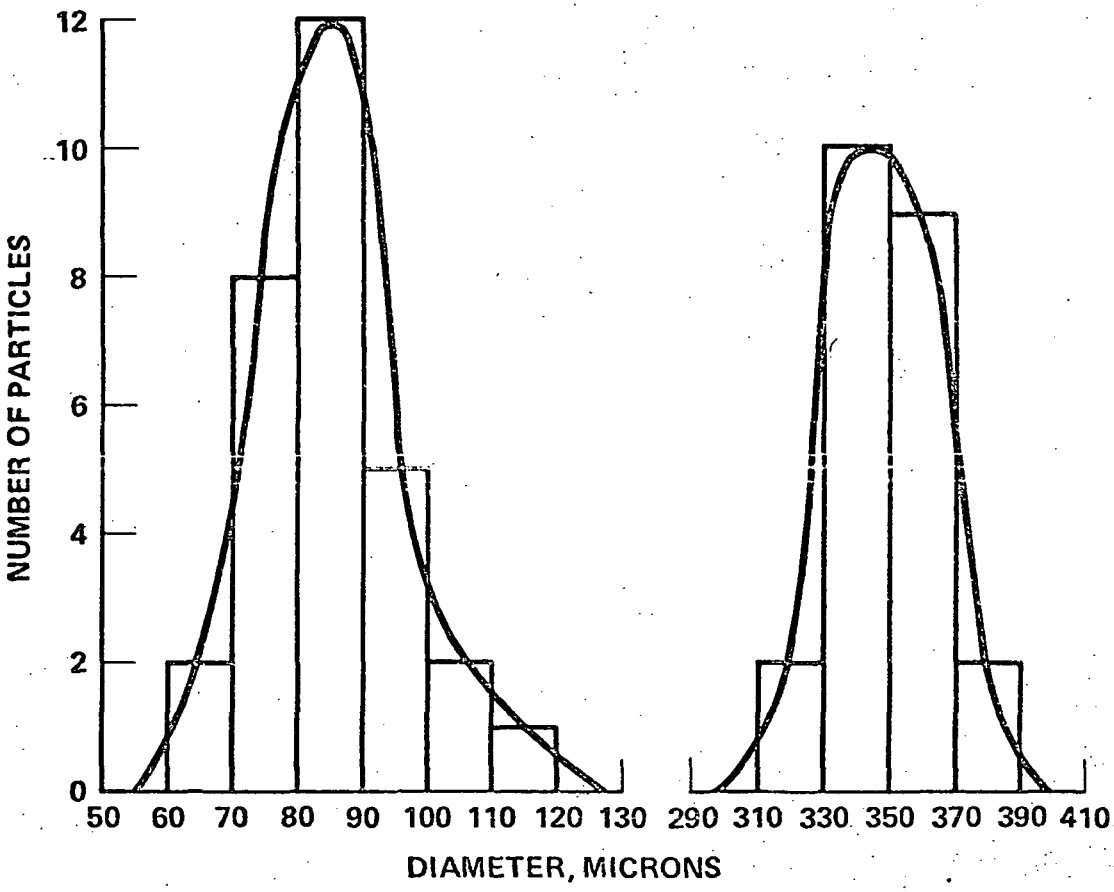

Figure 6. Typical particle size distributions.

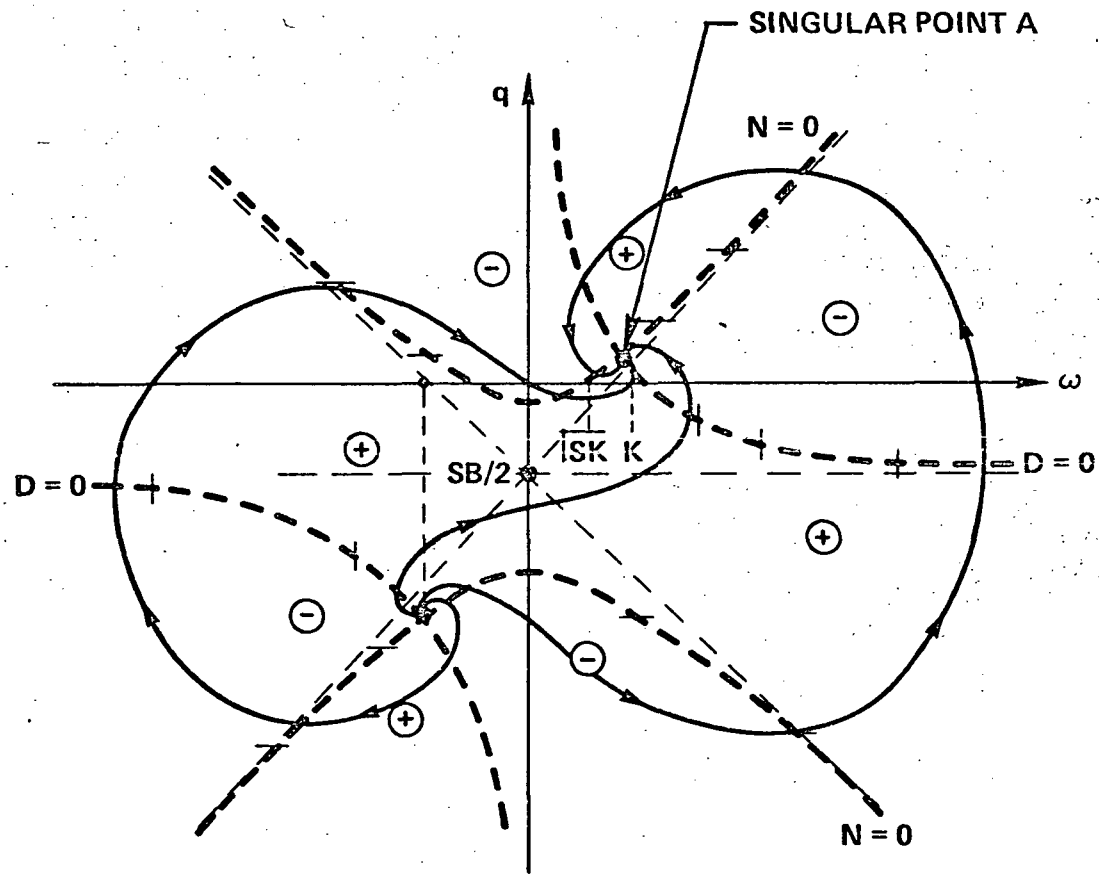

Figure 7. Character of the solutions for the motion of particles in a solid-body vortex.

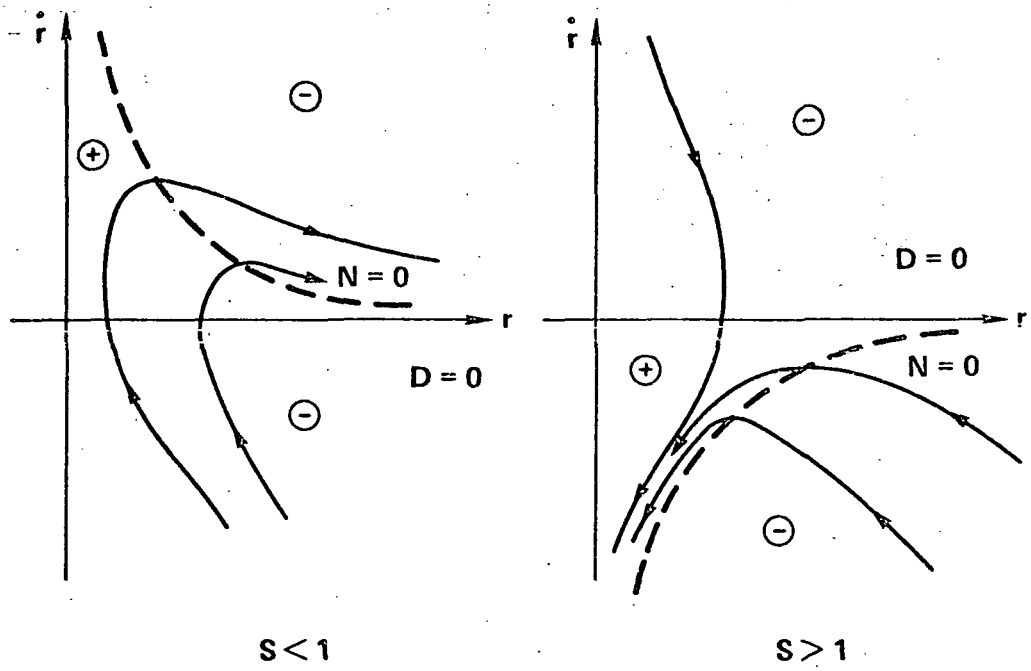

Figure 8. Characteristic trajectories of particles in a potential vortex.